Surface Restructuring of Nanoparticles: An Efficient Route for Ligand−Metal Oxide Crosstalk

T. Rajh,* L. X. Chen, K. Lukas, T. Liu, M. C. Thurnauer, and D. M. Tiede

Chemistry Division, Argonne National Laboratory, Argonne, Illinois 60439

Surface modification of nanocrystalline metal oxide particles with enediol ligands was found to result in altered optical properties of nanoparticles. The surface modification results in a red shift of the semiconductor absorption compared to unmodified nanocrystallites. The optical shift is correlated to the dipole moment of the Ti−ligand complexes at the particle surface and decreases with the ligand size. The binding was found to be exclusively characteristic of colloids in the nanocrystalline domain(<20 nm). X-ray near-edge structure measurements at Ti K edge indicate that in this size domain the surface Ti atoms adjust their coordination environment to form undercoordinated sites. These five-coordinated defect sites are the source of novel enhanced and selective reactivity of the nanoparticle toward bidentate ligand binding as observed using IR spectroscopy. Enediol ligands have the optimal geometry for chelating surface Ti atoms, resulting in a five-membered ring coordination complex and restored six-coordinated octahedral geometry of surface Ti atoms. The binding of enediol ligands is enhanced because of the stability gained from adsorption-induced restructuring of the nanoparticle surface. Consistent behavior was found for the three different nanocrystalline metal oxide systems: TiO_2, Fe_2O_3, and ZrO_2.

Introduction

Semiconductor particles that are in the nanometer size regime have attracted significant attention because of their atom-like size-dependent properties.[1−7] Whereas most studies have focused on the changes of the electronic properties due to the physical confinement of electrons and holes in potential wells defined by crystallite boundaries, little attention has been paid to the effects of surface modification and surface reconstruction on the electronic properties of nanoparticles. TiO_2 is a large band gap semiconductor with large electron effective masses (m_e^* ≈ 1),[8] and the physical confinement of electrons and holes (quantization effects) occurs only with small particle sizes (D < 25 Å).[9] Moreover, colloidal particles of TiO_2 can be controllably prepared in the size regime 25 < D < 300 Å, making them suitable for the investigation of surface effects in the nanocrystalline regime in the absence of change in electronic properties due to the electron and hole confinement effects.

Nanoparticles of TiO_2 have been intensively studied because of their potential unique applications in the photocatalytic clean up of water contaminated with hazardous industrial by-products[10−13] or as a photoactive material in nanocrystalline solar cells.[14−18] Titanium dioxide could be the catalyst of choice because it is cheap, nontoxic, and has redox properties that are favorable both for oxidation of many organic pollutants and for reduction of a number of metal ions or organics in aqueous solution. Excitation of TiO_2 with light energy greater than its band gap (3.2 eV) generates electron−hole (e^-/h^+) pairs that can be exploited in various processes at the particle interface. Photogenerated carriers migrate to the particle surface and participate in reduction and oxidation processes at the surface. Although TiO_2 is very effective from an energetic point of view, it is relatively inefficient as a photocatalyst with respect to

optimized photochemical systems such as natural photosynthesis. The main energy loss in all investigated particulate systems is due to the recombination of charges generated in the illumination of semiconductor particles, which is manifested as the relatively low efficiency of long-lived charge separation. Also, the use of TiO_2 for photocatalytic applications driven by solar light is limited because it has a wide band gap and thus absorbs fewer than 5% of the available photons of the solar spectrum. There has been tremendous interest in recent years in developing dye sensitization for the photoexcitation of TiO_2 in the visible region via photoinduced interfacial electron transfer.[14−19] Therefore, the main focus of research for the application of semiconductor-assisted photocatalysis is to improve both the separation of charges and the TiO_2 response in the visible spectral region.

Recently, we have reported a new route to improving the optical response of nanocrystalline TiO_2 in the visible spectral region. The approach involves direct electron transfer from ascorbate[20] and mercaptocarboxylic modifiers[21] of TiO_2 into the conduction band of nanocrystalline TiO_2 particles. Chelation of surface Ti atoms with electron-donating bidentate ligands in these systems changes the electronic properties of nanocrystalline particles. The binding of surface modifiers was found to be exclusively characteristic of small-particle colloids in the nanocrystalline domain and was stabilized by ligand-induced surface restructuring of the nanoparticle surface. Likewise, Rabani et al.[22] have reported a theoretical model for electronic properties of nanocrystalline particles that includes the effects caused by the presence of a dielectric medium. In their work, they predicted that large energy shifts (∼1 eV) of LUMO states are expected because of the formation of significant dipole moments in nanocrystalline particles. Herein, we report a whole class of enediol ligands that adjust the coordination geometry of the surface Ti atoms and shift the onset of absorption toward the visible region of the spectrum, compared to unmodified nanocrystallites. The same ligands were found to adjust the

* Corresponding author. E-mail: Rajh@anl.gov.

coordination environment and optical properties of nanocrystalline Fe_2O_3 and ZrO_2. Electron paramagnetic resonance (EPR) was used to obtain a molecular-level understanding of the origin of the direct charge transfer in these systems and the corresponding accepting and donating sites.

Experimental Section

All the chemicals used were reagent grade and were used without further purification (Aldrich or Baker). Nanopure® water was used. The pH was adjusted to 3.5 with NaOH or HCl. Oxygen was removed by bubbling with argon or nitrogen. The seeds of colloidal TiO_2 were prepared by the dropwise addition of titanium(IV) chloride to cooled water. The temperature and rate of component mixing of reactants were controlled by an apparatus developed for automatic colloid preparation.[21,23] The pH of the solution was between 0 and 1, depending on the $TiCl_4$ concentration. Slow growth of the particles was achieved by using dialysis at 4 °C against water until the pH of the solution reached 3.5, when particle growth was complete. Surface modification of TiO_2 resulting in the formation of a charge-transfer complex was achieved by the addition of surface-active ligands at concentrations required to cover all surface sites ($[Ti_{surf}] = [TiO_2]12.5/D^{24}$ is the molar concentration of surface Ti sites, $[TiO_2]$ is the molar concentration of TiO_2 in molecular units, and D is the diameter of the particle).

The seeds of colloidal Fe_2O_3 nanoparticles were prepared by thermal hydrodialysis of $FeCl_3$ in water.[25,26] Accordingly, the $FeCl_3$ solution was added dropwise to hot water, and the temperature and rate of component mixing of reactants were carefully controlled. Following the $FeCl_3$ hydrolysis, the solution was incubated at 75 °C for 24 h and then cooled to room temperature. The pH of the solution was between 1.2 and 1.8, depending on the $FeCl_3$ concentration. Analogous to the procedure developed for TiO_2 nanoparticles, the formation of seeds was followed by slow particle growth achieved by increasing the pH of the solution to 4 using dialysis at 4 °C.[21,23] A majority of the particles grow during dialysis because the solubility of iron oxide particles decreases from 0.01 M at pH 1.8 to 10^{-9} M at pH 4.[27] The concentration was controlled and determined using inductively coupled plasma (ICP) spectrometry to be in the range of 0.02–0.1 M. Ligating agents were added in amounts that would correspond to the formation of a monolayer on the nanoparticle surface. Surface-modified samples displayed an electron diffraction pattern of hematite with the same lattice parameters as those of unmodified samples. ZrO_2 nanoparticles were obtained via analogous procedures using $ZrOCl_2$ as a starting compound. The concentration of the ZrO_2 colloid was determined after dialysis (4500 mol wt cut off) using ICP to be in the range 0.06–0.1 M.

Apparatus. The absorption spectra were taken at room temperature in cells with 0.2-, 0.5-, and 1-cm optical path lengths using a Shimadzu UV-1601 UV/vis spectrophotometer. X-band EPR experiments were conducted on a Bruker ESP300E spectrometer equipped with a Varian cavity and a variable-temperature cryostat (Air Products) and a Varian E-9 EPR spectrometer equipped with a Varian cavity and a variable-temperature cryostat (Oxford) cooled to liquid helium temperature. The microwave frequency was determined after each measurement using a Hewlett-Packard 5352B frequency counter. Samples were excited using an Xe 300-W lamp (ILC) with the UV light removed by 400-nm cutoff filters. Samples were checked for background EPR signals before and after illumination. The g factors were calibrated for homogeneity and accuracy by comparison to a Mn^{2+} standard in a SrO matrix ($g = 2.0012$
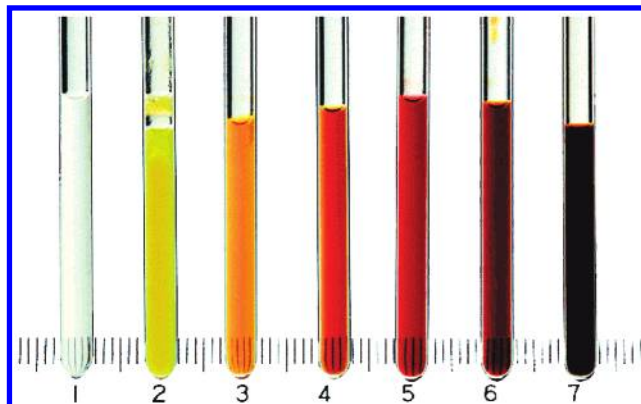
Figure 1. Surface-modified 45-Å TiO_2 nanoparticles with different bidentate ligands: (1) bare TiO_2, (2) salicylic acid, (3) dihydroxycyclobutenedione, (4) vitamin C, (5) alizarin, (6) dopamine, and (7) *tert*-butyl catechol. Molecule structures 2–7 are shown in Table 1.

± 0.0002)[28] and by using coal samples with $g = 2.00285 \pm 0.00005$,[29] respectively.

X-ray absorption near-edge spectra (XANES) and extended X-ray absorption fine structure (EXAFS) measurements were carried out at a wiggler beamline (11ID-D) and a bending magnet beamline (12 μ_B) of the Basic Energy Science Synchrotron Research Center, Advanced Photon Source at Argonne National Laboratory. Si 220 and 111 crystals were used in the double-crystal monochromator at the two beamlines, respectively. Details of the experiments are described elsewhere.[30]

FTIR. Measurements were performed on a Nicolet 510 Fourier transform infrared spectrometer equipped with a Spectra-Tech, Inc. diffuse reflectance accessory. The resolution was 4 cm^{-1}. All samples were 8 wt % of sample in a KBr matrix. Typically, 100 scans were performed for each spectrum. All results are presented as normalized Kubelka–Munk plots.

Results and Discussion

Optical Properties of Nanocrystalline TiO_2. When the metal oxide particles are in the nanocrystalline regime, a large fraction of the atoms that constitute the nanoparticle are located at the surface with significantly altered electrochemical properties. Because of the truncation of the crystal units at the surface and their weaker covalent bonding with solvent species compared to the bonding within the lattice, the energy level of the surface species is found in the midgap region, thereby decreasing their reducing/oxidizing abilities.[31] In addition, we have found that as the size of nanocrystalline TiO_2 becomes smaller than 20 nm the surface Ti atoms adjust their coordination environment from hexacoordinated (octahedral) to pentacoordinated (square pyramidal).[20] Using X-ray absorption spectroscopy, we also found that the change in coordination environment is followed by a compression of the Ti–O bond to accommodate for the curvature of the nanoparticle.[32] These undercoordinated defect sites are the source of novel enhanced and selective reactivity of the nanoparticle toward bidentate ligand binding. All of the investigated enediol ligands were found to undergo unique binding at the surface, resulting in new hybrid properties of the surface-modified nanoparticle colloids. These hybrid properties arise from the ligand-to-metal charge transfer (CT) interaction between the ligand and surface metal atoms that further couple with semiconductor electronic properties of the core of the nanoparticle. As a result, in these CT nanocrystallites, the onset of absorption is shifted to the red, as compared to that for unmodified nanocrystallites (Figure 1). This effect is opposite to the effects induced by the electron and hole confinement in

Surface Restructuring of Nanoparticles

J. Phys. Chem. B, Vol. 106, No. 41, 2002 **10545**
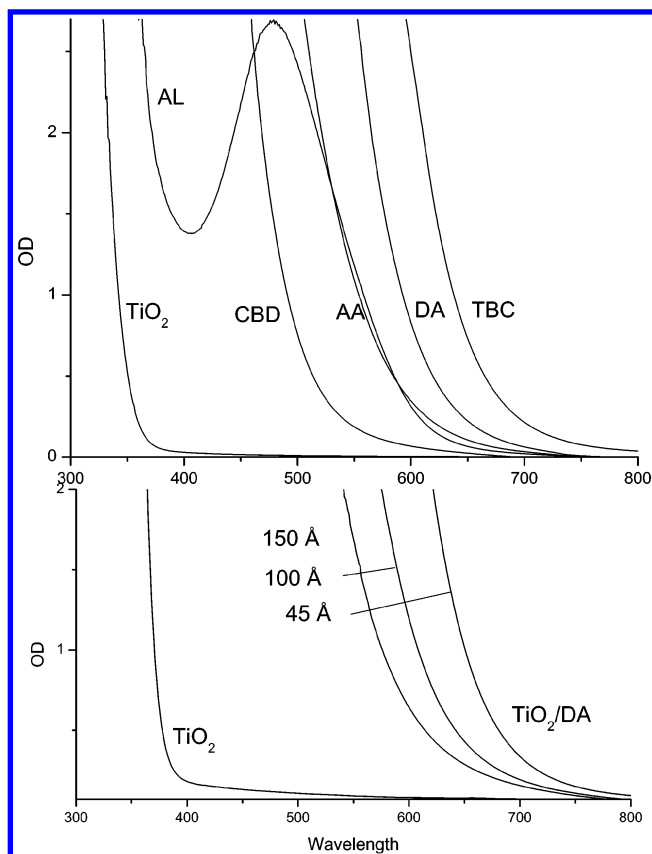
Figure 2. Absorption spectra of surface-modified (a) 0.3 M 45-Å TiO$_2$ (pH 3.5) with different enediol ligands—CDB, dihydroxycyclobutene-dione; AA, ascorbic acid; AL, alizarin; DA, dopamine; and TBC, *tert*-butyl-cathecol (optical path 0.2 cm) and (b) different particle sizes of 0.38 M TiO$_2$ modified with dopamine (optical path 0.5 cm).

Figure 3. Absorption spectra of the systems shown in Figure 2 but diluted by a factor of 10. The optical absorption spectra of the surface modifiers alone are also presented.

which an effective band gap is shifted to higher energies.[1-7,33] Coupling of these two effects can achieve exceptional fine-tuning of the optical and electrochemical properties of semiconductor nanoparticles.

The optical shift induced by surface modification was tuned by employing different surface-active enediol ligands ranging from a shift of 0.8 for salicylate (SA) to 2.0 eV for *tert*-butyl catechol (TBC) and is shown in Figure 2. The position of the absorption threshold for these surface-modified nanoparticles was found to shift according to the dipole moment of surface-bound Ti—ligand complexes (Table 1). Dipole moments were calculated by constructing bidentate complexes of enediol ligands with Ti having octahedral coordination (the residual four bonds were linked to oxygen atoms mimicking anatase lattice and terminated with hydrogens). Inducing the dipole moment on the surface involves shifting of the electronic charge inside the complex. The effect is analogous to that of "exciting the complex to some extent"[34] and consequently shifting the absorption edge. Apart from the shift in the absorption edge, the optical properties for monocyclic aromatic enediol-modified semiconductor nanoparticles paralleled the absorption properties characteristic of the band structure in semiconductor nanoparticles, having a continuous rise of absorption toward higher energies (Figure 3a). We attribute the shift in the absorption edge in the modified semiconductor nanoparticles to the excitation of localized electrons from the surface modifier into the conduction band continuum states of the semiconductor particle.[20] A similar red shift but localized charge-transfer complex resulting in an absorption spectrum with a charge
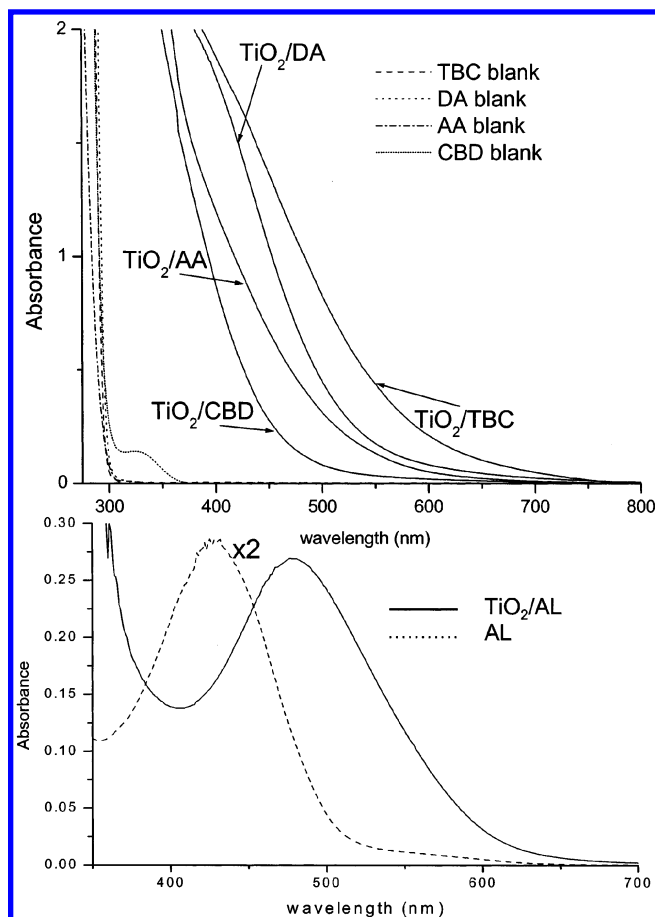
maximum at 390 nm was previously observed for Ti^{4+} and catechol molecules.[35]
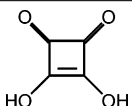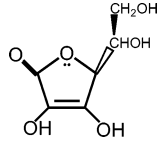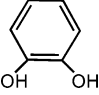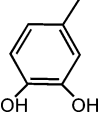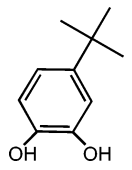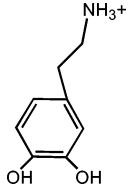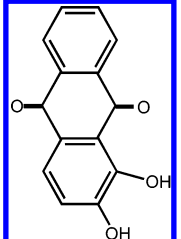
In contrast to the generally simple shift in the position of the absorption edge in the case of monocyclic enediol-modified nanocrystalline semiconductors, the optical properties of nanoparticles modified with polycyclic aromatic ligands showed a more complex spectrum and a smaller shift in the absorption threshold than expected from the dipole moments of surface-bound complexes. These properties are demonstrated with alizarin (AL)-modified TiO$_2$ nanoparticles (Figures 2 and 3b). The absorption spectrum for AL—TiO$_2$ showed a clear absorption maximum near 500 nm that is suggestive of an excitation to a localized state rather than excitation to a continuum. Similar results were obtained recently by Huber et al.[36] In this work, the authors investigated the mechanism of electron injection from alizarin into TiO$_2$ with ultrafast optical spectroscopy and concluded that surface states play a significant role in the electron-transfer mechanism.

Figure 2b shows absorption spectra of different particle sized TiO$_2$ colloids modified with dopamine (DA). The onset of absorption does not change with the particle size, but the overall absorption is enhanced with decreasing particle size. The change of the intensity of absorption was found to be proportional to the fraction of the surface Ti atoms and correlates with the number of surface sites in nanocrystalline TiO$_2$.

Optical Properties of Nanocrystalline Fe$_2$O$_3$ and ZrO$_2$. We have explored undercoordination of surface atoms as a general feature of nanocrystalline materials that results in enhanced reactivity at the surfaces of nanocrystalline metal oxides. For that purpose, surface modification of three different

TABLE 1: Enediol Ligands Used for Surface Modification of 45 Å TiO$_2$ and the Change of Their Dipole Moments and Optical Shifts upon Binding to Surface Ti Sites[a]

| ligand	label	structural formula	dipole moment of Ti−ligand complex (Debye)[b]	$10^4 \Delta g$	ΔE_g (eV)
dihydroxy cyclobutenedione	CBD		7.65	47	0.8
ascorbic acid	AA		9.7	28	1.2
catechol	CAT		12.57	17	
methyl catechol	MetCAT		14.0	13	
tert-butyl catechol	TBC		15.2	19	2.0
dopamine	DA		16.1	16	1.9
alizarin	AL		14.7	5.4	1.4

[a] g values of the radical cations produced by illumination of corresponding CT nanoparticles are also listed as a measure of their aromatic character. [b] Dipole moment calculations were performed with HyperChem software, a product of Hypercube Inc., using the ZINDO/1 semiempirical method for determining the structures of complexes containing transition metals in a single-point calculation. The program was tested with molecules of known dipole moments. The conformations of the modifier that were used for calculations were the ones suggested by IR studies.

metal oxides having different crystalline structures, band gaps, and Fermi level positions (proportional to electron affinity of the semiconductor (χ), the Helmholtz layer potential drop at the semiconductor interface (V_H), and the difference between the Fermi level and the majority carrier band edge (ΔE_F))[31] were investigated. Fe$_2$O$_3$ is a semiconductor with a closed-packed hexagonal structure having a larger electron affinity $\chi_{Fe_2O_3}$ (E_{cb}= 0.44 V vs NHE at pH 4) and a smaller band gap (E_g=2.0 eV) than TiO$_2$ (E_{cb}= −0.17 V at pH 4, E_g = 3.2 eV). ZrO$_2$, however, has a cubic structure and a smaller electron affinity χ_{ZrO_2} and a larger band gap (E_{cb}= −1.32 V at pH 4, E$_g$=5 eV) than TiO$_2$.[31] Surface modification of Fe$_2$O$_3$ and ZrO$_2$ with enediol ligands also led to a change of the optical properties (Figure 4). Again, the onset of absorption is shifted to the red, as compared to that of unmodified nanocrystallites.

Because of the small band gap, unmodified Fe$_2$O$_3$ nanoparticles have an onset of absorption at 600 nm. The onset of absorption of surface-modified particles was shifted to the IR part of the spectrum and could not be accurately determined in aqueous solution because of the water absorption in this part of the spectrum. We used diffuse reflectance spectroscopy to determine the onset of absorption of dried samples. The effective band gap of dopamine-modified 60 Å Fe$_2$O$_3$ was determined to be 0.89 eV, 1.12 eV for ascorbate, and 1.40 eV for alizarin. These shifts (ΔE of 0.6 eV for alizarin, 0.88 eV for ascorbate, and 1.11 eV for dopamine) are somewhat smaller than the shifts obtained in TiO$_2$ samples (Figures 2 and 4). This is consistent with the larger electron affinity $\chi_{Fe_2O_3}$ compared to χ_{TiO_2}. Figure 4c depicts the energy-level positions in the three investigated metal oxide colloids after surface modification obtained from the shifts of the absorption thresholds. These results indicate that the electrochemical potentials (μ) of DA, AA, and AL at TiO$_2$ and Fe$_2$O$_3$ surfaces are similar.

Surface Restructuring of Nanoparticles

J. Phys. Chem. B, Vol. 106, No. 41, 2002 **10547**

SCHEME 1: Plausible Alizarin Structures on the Surface of ZrO_2
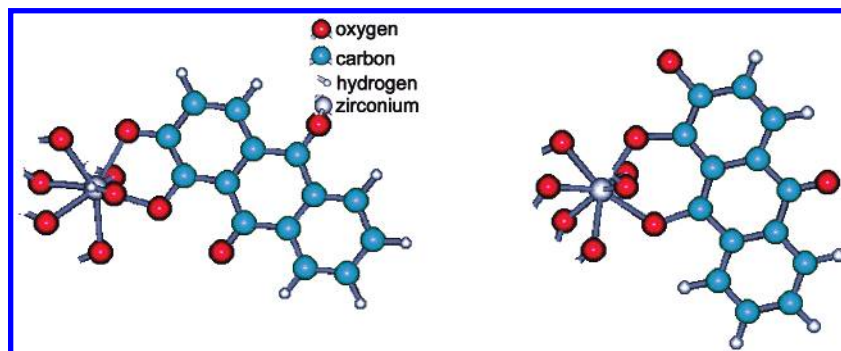
ZrO_2 colloids experience a similar red shift upon surface modification. Upon surface modification, the effective band gap of ZrO_2 was decreased 1.6 eV for AA and 1.7 eV for DA. These shifts are comparable to the optical shifts obtained for TiO_2, although one would expect larger shifts because of the smaller electron affinity of ZrO_2 compared to that of titanium dioxide. However, surface modification of ZrO_2 with alizarin results in unexpectedly large shifts of 3 eV, suggesting effective electronic coupling between alizarin and ZrO_2 surface atoms. Better coupling of alizarin in ZrO_2 may come from the structure of alizarin that allows the formation of a six-membered ring at the nanoparticle surface (Scheme 1). This structure is formed by one of the resonant structures of alizarin that involves an oxygen from the central ring. In that structure, an oxygen bonded to the central ring in keto form binds to the surface Zr atom simultaneously with one of the OH groups, while the other OH group turns into the keto form. This binding motif results in six-membered ring chelates of the surface Zr atoms. A six-membered ring has larger bond angles that can accommodate the cubic structure of ZrO_2. Whereas both TiO_2 and α-Fe_2O_3 are composed of hexagonal TiO_6 and FeO_6 clusters in distorted O_h symmetry, ZrO_2 is composed of ZrO_8 cubic clusters with bond angles differing from the bond angles of five-membered rings formed by mononuclear aromatic enediol chelating complexes. Weaker coupling of the monocyclic aromatic enediol ligands in ZrO_2 might be caused by the smaller overlap of ligand orbitals with eight-coordinated zirconium. Surface modification of ZrO_2 with alizarin also results in the absorption spectrum that suggests localized ligand-to-metal charge transfer that is probably due to the weaker coupling of the modified Zr surface atoms to the nanoparticle lattice atoms.
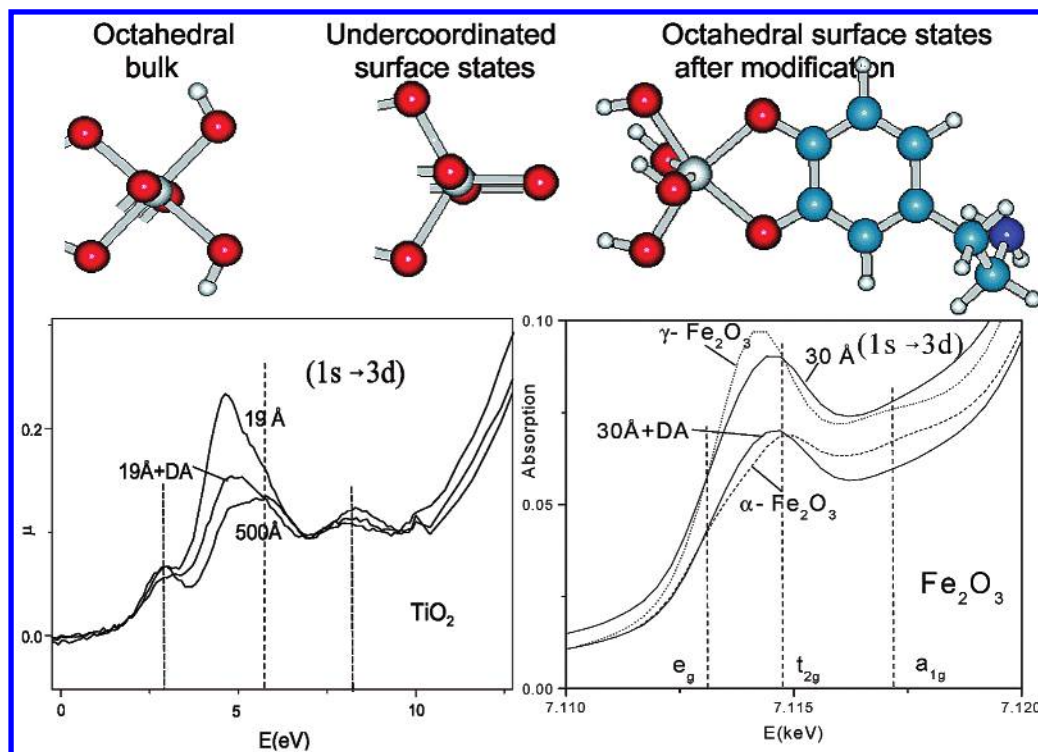
Crystal Structure of Surface Sites in Nanocrystalline Metal Oxides. The stability of the chelating complex at the nanoparticle surface is enhanced because of ligand-induced restructuring of the nanoparticle surface demonstrated by the changes in both XANES and EXAFS upon surface modification. Both of these spectroscopies reveal the existence of undercoordinated sites at the particle surface for all three investigated metal oxide nanoparticles. We have found previously using XANES spectroscopy that AA surface modification results in restoration of the particle surface defect sites into an octahedral coordination environment.[20,32] Both XANES and EXAFS spectra of nonmodified TiO_2, Fe_2O_3[30] (Figure 5), and ZrO_2[37] nanoparticles confirmed that the surface of the nanoparticles is composed of undercoordinated metal binding sites. These undercoordinated sites were removed upon binding of monocyclic aromatic enediol ligands (CBD, AA, and DA) to the surface of the nanoparticle, which in turn restored the pre-edge features of bulk metal oxides.
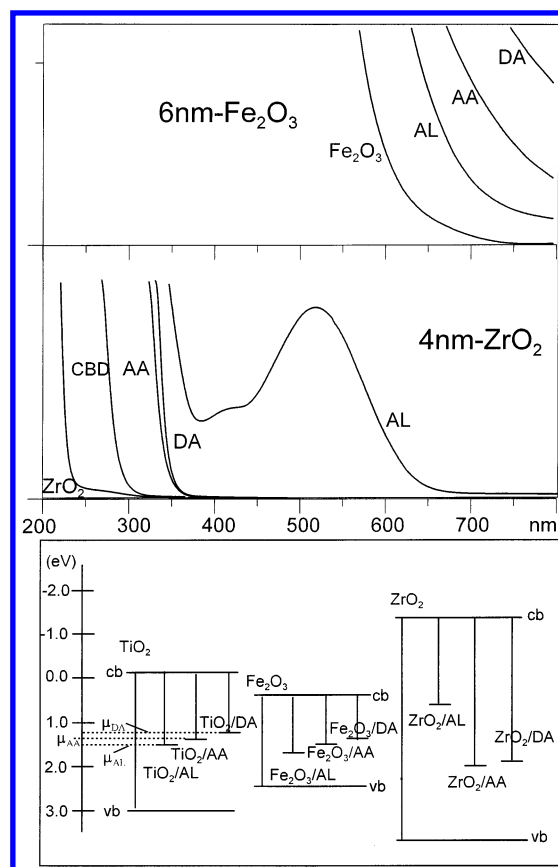
Figure 4. Absorption spectra of surface-modified (top) 0.1 M 60-Å Fe_2O_3 (pH 4) and (middle) 40 Å ZrO_2 (pH 4) with different enediol ligands in conjunction with (bottom) an energy-level scheme associated with surface modification of the investigated metal oxide nanoparticles.

TiO_2 particles in the small-particle regime have an anatase structure where every titanium cation is surrounded by six oxygen atoms in elongated octahedron geometry (D_{2d}). Because of the resultant crystal field, the 3d levels of Ti^{4+} that form a conduction band of TiO_2 are split into t_{2g} and e_g sublevels. The unequal length of the six Ti−O bonds produces a splitting of the t_{2g} and e_g orbitals into two subsets. Symmetry considerations show that the 4p orbitals of the central Ti atom mix with the 3d orbitals of neighboring Ti atoms and that the 3d−4p hybridized subbands form a conduction band of anatase TiO_2, which is found experimentally in the pre-edge structure of the XANES spectrum of TiO_2.[38]

The pre-edge structure of nanocrystalline TiO_2 in the size domain of <200 Å shows changes in spectral features from those of bulk TiO_2. The changes become more pronounced as the size of the nanoparticle becomes smaller, suggesting that

Figure 5. Pre-edge structure of XANES spectrum of TiO_2 and Fe_2O_3 before and after surface modification with DA in conjunction with spectra of corresponding polycrystalline samples.

the change in crystal structure of surface atoms induces changes in electronic structure. Because of the change of symmetry of the surface sites, the overlap of the orbitals of the metal atoms with those of neighboring atoms changes, and hybridized subbands that form the conduction bands of metal oxides depart from the electronic structure of the bulk. This is displayed by the changes of the pre-edge structure in the XANES spectra of metal oxides. Upon binding with enediol ligands to the surface sites, the asymmetry of the these sites is removed, and the bulk structure of the conduction bands is restored.[38] This is manifested by the reconstruction of the pre-edge features of bulk metal oxides.

Surface Structure of Enediol Ligands at the Nanoparticle Surface. Using FTIR spectroscopy, we have confirmed bidentate binding in all investigated enediol ligands. As an example, a diffuse reflectance spectrum of catechol-modified TiO_2 is shown in Figure 6 in conjunction with unmodified TiO_2 and catechol. The infrared spectrum $(4000-1000$ cm$^{-1})$ of colloidal TiO_2 consists of three absorption bands: (1) a narrow band at 3650 cm^{-1} associated with the vibration of OH groups linked to surface Ti atoms, (2) a broad absorption band $(3700-2600$ cm$^{-1})$ centered at 3200 cm^{-1}, which is the characteristic frequency for the hydrogen-bonded OH stretching vibration, and (3) a narrower band at 1620 cm^{-1}, which is associated with the scissoring vibration of adsorbed water molecules.[39] Adding catechol results in the replacement of surface OH groups and the coordination of surface Ti atoms with both OH groups of catechol. This is demonstrated in the FTIR spectrum by the disappearance of the stretching vibration of OH groups of TiO_2 at 3650 cm^{-1} as well as the disappearance of both stretching (3450 cm^{-1} for intramolecular hydrogen-bonded hydroxyl groups and 3350 cm^{-1} for intermolecular hydrogen-bonded hydroxyl groups) and bending vibrations of catechol OH groups
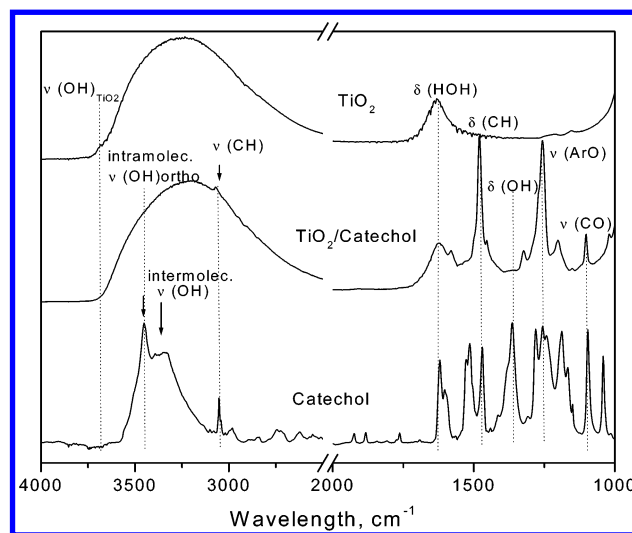
Figure 6. Adsorption of catechol on a 45-Å TiO_2 colloid. Infrared spectra of dried samples of (bottom) catechol, (middle) 0.1 M cathecol-modified 0.3 M TiO_2 colloid at pH 4 dried and thoroughly washed with CH_3OH, and (top) dried 0.3 M TiO_2 colloid at pH 4.

at 1365 cm^{-1}. It should be noted that stretching and bending vibrations of the CH groups of catechol (3050 and 1480 cm^{-1}, respectively) as well as aryl oxygen stretching at 1250 cm^{-1} were not affected by catechol adsorption on the TiO_2 surface. [40] This bidentate binding with ortho hydroxyl groups of enediol ligands suggests the formation of a five-membered ring around surface Ti atoms, which is a favorable conformation of bond angles and distances for the octahedral coordination of surface Ti atoms. Calculations of small clusters indicate that when catechol dissociatively chemisorbs on the edge or corner site a bidentate structure is favored by $4-6$ kcal/mol compared to molecular adsorption.[41] These calculations also indicate that

Surface Restructuring of Nanoparticles

J. Phys. Chem. B, Vol. 106, No. 41, 2002 **10549**
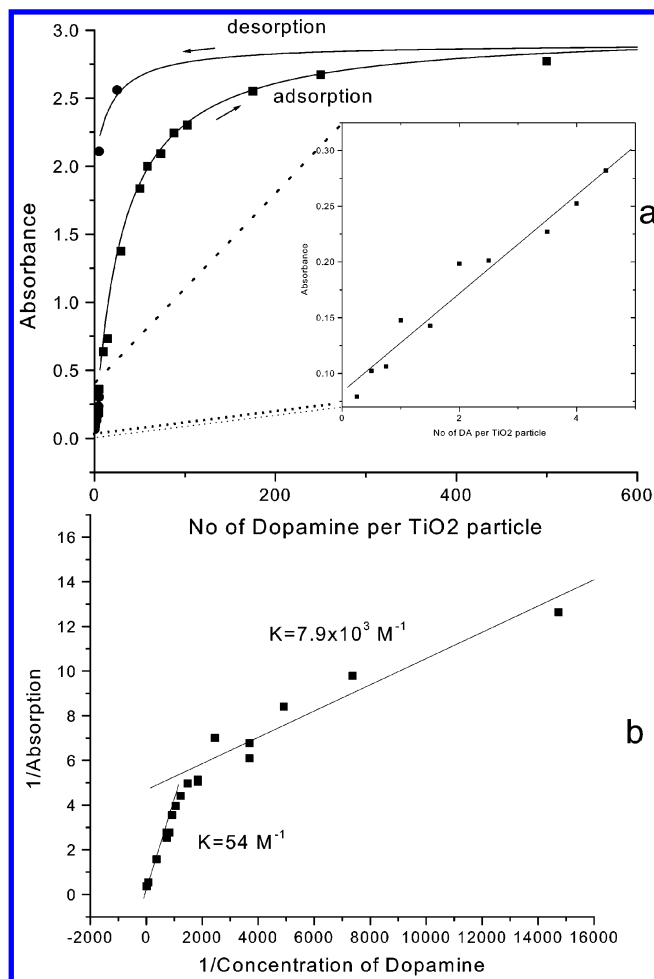
Figure 7. (a) Adsorption and desorption of DA from the surface of 0.38 M 45-Å TiO$_2$ measured from the absorption of CT nanoparticles at 575 nm, optical path length 0.5 cm. Data obtained for the adsorption curve were recorded 2 h after surface modification. Desorption data were obtained by dialysis of DA-modified TiO$_2$ against water in the volume ratios 1:20 and 1:100, equilibrated for 4 days, and recorded. Inset: Measurement of absorption changes due to formation of CT nanoparticles at small surface coverage. (b) Linear dependence of inverse concentration of CT nanoparticles on inverse concentration of DA. Two slopes indicate the existence of two binding sites having different free energies of adsorption.

dissociative chemisorption of catechol leads to a shift of opticaltransitions to longer wavelengths in the optical spectrum, whereas molecular adsorption does not.

Surface modification of TiO$_2$ colloids with catechol resulted in "gelling" of the solution. This is the consequence of enhanced particle−particle interaction because surface modification with catechol eliminates the surface charge. Surface modification with DA ligands having terminal amino group ($-NH_3^+$) allows for particle−particle repulsion and leads to a very stable colloidal solution for pH < 6. This property can be used for selective precipitation of TiO$_2$ in aqueous solution.

The binding of the DA ligand follows the Langmuir-type adsorption isotherm (Figure 7). Because these novel charge-transfer semiconducting materials exhibit optical properties that are distinct from their constituents, Benesi−Hildebrandt analysis for molecular complexes can also be employed to determine the stability constant of the complex.[42] Although the Langmuir isotherm is used for bulk catalysts and Benesi−Hildebrandt analysis is used for molecular complexes, for small particles

both approaches lead to the same relationship between the stability constant and concentration of the CT nanoparticles. For a solution of 45-Å TiO$_2$ colloids containing 1.7×10^{-4} M of particles and 405 surface titanium sites per particle, one can consider[43]

$$\text{Ti}_{\text{surface}} + \text{DA} \rightleftharpoons \text{CT}_{\text{complex}} \quad (1)$$

For Benesi-Hildembrandt equilibrium:

$$K = \frac{[\text{CT}]}{[\text{Ti}][\text{DA}]} \quad (2)$$

$$[\text{CT}] = A/\epsilon l \quad (3)$$

$$\frac{l}{A} = \frac{1}{\epsilon K[\text{Ti}]} \frac{1}{[\text{DA}]^o} + \frac{1}{\epsilon[\text{Ti}]} \quad (4)$$

For Langmuir adsorption isotherm:

$$k_a[\text{DA}]N(1-\theta) = k_d N\theta, \ \theta = [\text{CT}]/[\text{CT}]_{\text{max}} \quad (2a)$$

$$\theta = K[\text{DA}]/1 + K[\text{DA}] = A/A_{\text{max}}, \ K = k_a/k_d \quad (3a)$$

$$\frac{1}{A} = \frac{1}{KA_{\text{max}}} \frac{1}{[\text{DA}]} + \frac{1}{A_{\text{max}}} \quad (4a)$$

where K is the equilibrium constant; k_a and k_d are rates of adsorption and desorption, respectively; [CT], [Ti], and [DA] are the concentration of the CT nanoparticles with dopamine, the concentration of surface Ti sites, and the concentration of dopamine, respectively; A and A_{max} are the absorbance values of a CT complex for a given and a saturation concentration of DA, respectively; ϵ is the extinction coefficient of the CT nanoparticles; and l is the optical path length. Both approaches lead to the same linear dependence of $1/A$ versus $1/[\text{DA}]$, and from the ratio of the intercept and the slope, the rate constants are determined. The adsorption approach has been used previously to determine the stability constants as well as the free energy of adsorption of catechol on TiO$_2$ particles in the size regime 13−400 nm, which was determined to be in the range -9.0 kcal/mol $< \Delta G° < -6.8$ kcal/mol.[44−46] Using the data for the adsorption of DA on the TiO$_2$ surface presented in Figure 7, a very similar value of -7.6 kcal/mol was obtained. However, using dialysis, we were able to investigate equilibrium concentrations of DA upon desorption of DA from the particle surface. The desorption of DA from the surface, however, did not follow the same behavior as adsorption (Figure 7). This indicates that there is a difference between the rates of adsorption and desorption. This difference additionally confirms bidentate binding of the surface modifier that stabilizes the complex because of the chelating effect, previously described in the work of Parkinson et al.[47] Both the Benesi−Hildebrandt and Langmuir isotherm methods described above require equilibrium conditions in which the rates of adsorption and desorption are equal. Therefore, determination of the binding constant from only the adsorption curve leads to underestimation of the stability constant as well as the absolute value of the free energy of adsorption, so we were not able to determine ΔG. Nevertheless, we were able to determine the existence of two binding sites with different free energies of binding (Figure 7b). The plot of the rate of adsorption versus DA concentration is composed of two distinct areas: the first applied to the initial bindings up to five dopamine molecules per particle, and the second, to the additional $\sim$320 DA per particle. A monolayer of 325 DA per particle corresponds to a surface area of 19.6 Å^2 occupied by
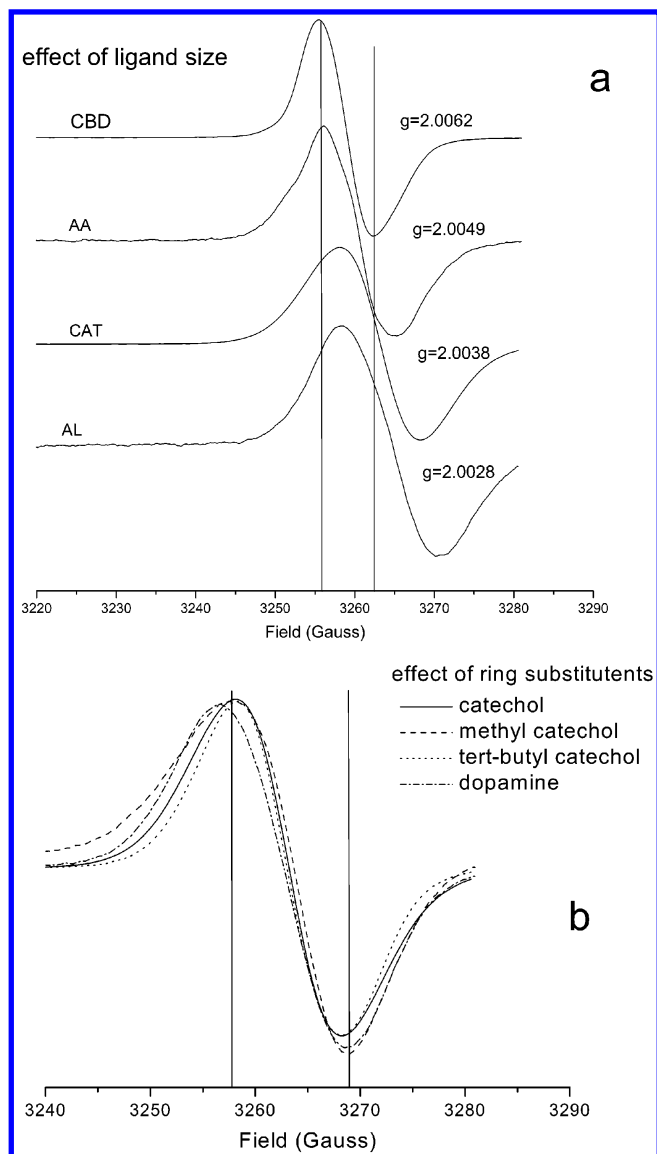
Figure 8. EPR spectra of photogenerated radical cations observed from the illumination ($\lambda > 400$ nm, 10 K) of 0.3 M surface-modified 45-Å TiO$_2$ colloids (a) with different number of π electrons and (b) with different pendant chains. Microwave power 0.5 mW, modulation amplitude 2 G, time constant 0.1, field scan 400 G.

each dopamine ligand. This surface area is comparable to the surface area 15.7 Å^2 [48] that is occupied by each Ti atom at the surface of anatase, indicating that practically every surface Ti atom acts as a binding site for dopamine adsorption and that 80% of the surface is covered with DA ligands. The remaining 20% of the Ti sites are not chelated, probably because of the steric hindrance of neighboring DA molecules. It should be noted that the stability of the dopamine-surface Ti atoms is larger than the stability of carboxyl (alanine, arginine), phosphono (amino phosphono propionic acid, amino phosphonic acid, TOPO), silane (phenylsilane, aminopropyltrimethoxysilane), or glycidyl (glycidol, glycidil isopropyl ether, 1,4-butanediol diglycidil ether) compounds with surface Ti atoms. Dopamine readily replaces these other surface modifiers from the TiO$_2$ nanoparticle surface, which is manifested by the appearance of a colored solution due to the formation of CT nanocrystallites. It should be noted that all investigated enediol ligands are by themselves extremely susceptible to oxidation. They decompose when adsorbed monodentately on large-particle TiO$_2$.[49] Apparently, because of the bidentate binding to nanoparticles, enediol

ligands gain stability and are not easily oxidized. As a consequence, dopamine- and ascorbate-modified TiO$_2$ colloids preserved their optical properties even after exposure to thousands of 10-mJ laser pulses[50] and daylight for 2−3 years. The only way we were able to cause decomposition of enediol ligands bound to the TiO$_2$ nanoparticle surface was by reaction with reducing radicals capable of hydrogen abstraction (methanol- and ethanol-free radicals).[51] In this case, bleaching of the charge-transfer absorption was observed to be proportional to the concentration of the reducing radicals.

Interfacial Charge Separation. The strong electronic coupling of enediol chelating ligands to nanocrystalline particles, which is a consequence of adsorption-induced surface restructuring, also affects the light-induced charge separation. Because the optical properties of modified particles are different from the optical properties of both constituents (Figure 3), optical transitions that occur are the consequence of the charge transfer between the two components. Using continuous wave (CW) EPR at cryogenic temperatures, we were able to establish the identities of the radical species formed by excitation ($\lambda > 500$ nm) of the charge-transfer complex of 45 Å TiO$_2$ nanoparticles with enediol modifiers. The shape and the width of the signal in the region $g > 2$ are dependent on the surface modifiers used for adsorption-induced restructuring of the surface, suggesting that the primary trap for photogenerated holes is localized at surface modifiers (Figure 8). The EPR signal broadens as the size of the ligand increases, mainly because of the increasing number of hydrogen atoms in the ligand, ranging from ΔH_{pp} of 7 G for CBD to ΔH_{pp} of 12.3 G for AL (Figure 8). The EPR spectra of catechol-based compounds were consistent with the spectra and hyperfine structure of the corresponding radical species formed in their complexes with metal ions.[52] There is an apparent g shift as the number of π electrons increases, indicating that electrons in conjugated systems become more delocalized, therefore shifting the g value toward that of the free electron ($g = 2.00232$), reaching $g = 2.0028$ for alizarin (Table 1). This observation is consistent with previously published behavior of aromatic radical species in which the g shift is proportional to the number of delocalized electrons in the π orbital of aromatic hydrocarbons.[53,54] However, this linear trend of increased π conjugation does not translate to the trends in the optical shift. Alizarin shifts the optical spectrum moderately, even though it has the largest number of π electrons and the largest g shift in the EPR spectrum of all investigated surface modifiers. These results suggest that the number of π electrons is not the only factor influencing the optical shift, but their distribution with respect to the nanoparticle surface is also an influence. Also, when H atoms in a side chain of surface modifiers are substituted with other nuclei, the line width of EPR spectra changes, but an apparent g shift is not observed. Surface modification with *tert*-butyl catechol (TBC), however, produces the largest optical shift of all the investigated ligands. The EPR spectrum of nonilluminated TBC-modified TiO$_2$ exhibiting relatively strong signals of the TBC radicals suggests that there is a ground-state charge exchange between the ligand and nanoparticle. Illumination leads to the simultaneous 2-fold increase of the signal intensity of the TBC radical and the appearance of the Ti(III) signal, indicating light-induced charge separation in which a hole is localized on the TBC modifier and electrons, on TiO$_2$ nanoparticles.

Illumination of surface-modified nanoparticles with all the investigated ligands also resulted in the appearance of two signals that are well resolved in the parallel orientation observed in the region $g < 2$. These signals are characteristic of radicals

Surface Restructuring of Nanoparticles

J. Phys. Chem. B, Vol. 106, No. 41, 2002 **10551**
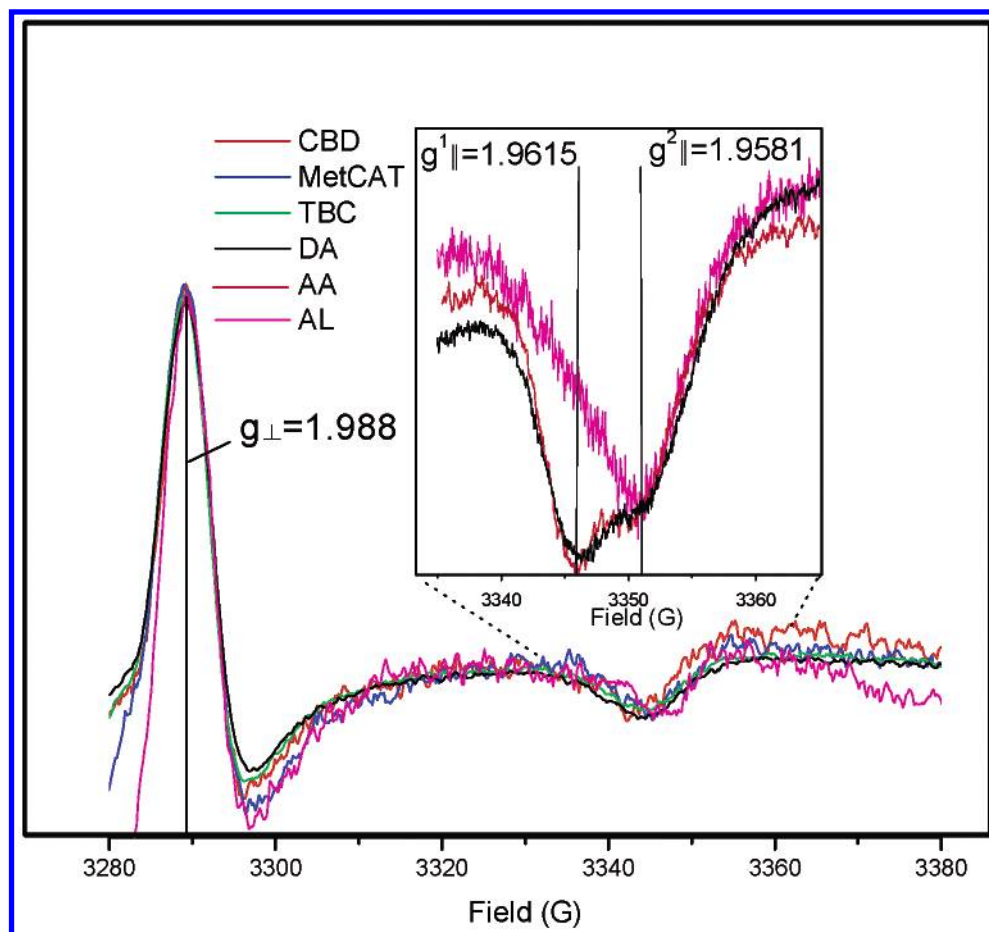
Figure 9. (a) EPR spectra of photogenerated electrons observed as Ti(III)$_{latt}$ centers observed from the illumination ($\lambda > 400$ nm, 10 K) of 0.3 M surface-modified 45-Å TiO$_2$ colloids that were surface-modified with different enediol ligands. Microwave power 0.5 mW, modulation amplitude 2 G, time constant 0.1, field scan 400 G. (b) Parallel component for AA-, DA-, and AL-modified samples recorded at a narrower field scan of 40 G and microwave power of 2 mW.

in which the unpaired electron occupies the d orbitals of lattice Ti atoms having an angular momentum component due to the spin−orbit coupling causing negative deviation from free-electron spin values ($g = 2.0023$) (Figure 9).[55−57] The signals are very narrow, with $g^1_{\parallel} = 1.9615$, $g^1_{\perp} = 1.9885$, $g^2_2 = 1.9581$, $g^2_{\perp} = 1.988$, and $\Delta H_{pp} = 2.5$ G. It has been found that electrons in anatase TiO$_2$ become easily self-trapped in the bottom of conduction bands that are dominantly d$_{xy}$ orbitals that are not filled after photoexcitation because the transitions from the top of valence band p$_{\pi}$ states to these states are dipole-forbidden.[8] The signal with a parallel component at higher field ($g = 1.9581$) was identified with a lattice-trapped Ti^{3+} ion. Meanwhile, the narrow component at $g = 1.9615$ tentatively was associated with a signal that was motionally narrowed by an electron hopping from one center to another.[20] A similar signal has been observed from partially reduced rutile TiO$_2$ and attributed to an electron loosely bound to an interstitial titanium ion or a completely delocalized electron.[58] However, self-trapping of photogenerated electrons at shallow restructured Ti surface sites having a slight difference in structure compared to their bulk structure cannot be ruled out. Our future research will address these issues by using femtosecond IR spectroscopy. Careful investigation of the parallel component in three different systems is shown in the inset of Figure 9. Photogenerated electrons in DA- and AA-modified particles show both localized and partially delocalized sites, whereas AL modification results in a molecular charge-transfer complex that leads to electron transfer to the localized Ti sites only. Parallel measurements of

optical absorption spectra show excitation of electrons in the delocalized conduction band for DA- and AA-modified particles, whereas the optical spectra of AL-modified samples show absorption maxima indicating a localized LMCT band. We were able to determine activation energies for electron localization by investigating the temperature dependence of the parallel component of the Ti(III) signal formed in steady-state illumination at 4.2 K of DA- and AA-modified TiO$_2$ particles. There is an activation energy for electron localization, and at 30 K, the motionally narrowed signal associated with the delocalized electron decreases in intensity, while the signal associated with localized trapped electrons increases in intensity, suggesting conversion of delocalized electrons into localized Ti(III) sites. This temperature corresponds to an activation energy of 2.6 meV. This energy is too small to prevent direct excitation from alizarin to the delocalized band of TiO$_2$, especially at room temperature, when kT exceeds the activation energy. Therefore, it is more likely that the structure of the surface sites restored with AL is different from that restored with the other ligands. Similar conclusions indicating the crucial role of surface sites in the electron injection mechanism of excited electrons from alizarin to wide band gap semiconductor colloids were drawn recently from ultrafast optical spectroscopy measurements.[36]

Conclusions

All enediol ligands form charge-transfer complexes with metal oxide nanoparticles, which results in a significant change in the nanoparticles' optical properties. The change of optical absorp-

tion spectra and the effective band gap of nanoparticles were found to be proportional to the density of delocalized π electrons and the dipole moment of surface-bound titanium enediol ligand complexes. Therefore, by varying surface modifiers only, the electronic properties of a particle can be tuned for frequency-selective photochemistry. This effect decreases the effective band gap of nanoparticles and is opposite to the quantization effect. The combination of selected surface modification with size quantization effects leads to an integral effect that can result in fine-tuning of the electronic properties of metal oxide semiconductors that show quantization effects at reasonable particle sizes (e.g., ZnO[59]). These systems also have an important feature: upon illumination, charge pairs are instantaneously separated between the donating organic modifier and the conduction band of metal oxides. Furthermore, the charge separation is reversible at low temperatures, indicating exceptionally shallow trapping of separated charge pairs. This fact designates the ligands as *conductive leads* that allow electronic linking of the nanoparticle into molecular circuits. When the ligands are covalently linked (wired) to electron-donating moieties, photoinduced electron transfer can be further extended, ultimately leading to a stabilized charge separation.

References and Notes

(1) Alivisatos, A. P. *Science (Washington, D.C.)* **1996**, *271*, 933.
(2) Bawendi, M. G. *NATO Adv. Study Inst. Ser., Ser. B* **1995**, *340*, 339.
(3) Brus, L. *Appl. Phys. A* **1991**, *A53*, 465.
(4) Henglein, A. *Chem. Rev.* **1989**, *89*, 1861.
(5) *Semiconductor Nanoclusters: Physical, Chemical and Catalytic Aspects*; Kamat, P. V.; Meisel, D., Eds.; Elsevier: Amsterdam, 1997; Vol. 103.
(6) Micic, O. I.; Nozik, A. J. *J. Lumin.* **1996**, *70*, 95.
(7) Rajh, T.; Peterson, M. W.; Turner, J. A.; Nozik, A. J. *J. Electroanal. Chem. Interfacial Electrochem.* **1987**, *228*, 55.
(8) Asahi, R.; Taga, Y.; Mannstadt, W.; Freeman, A. J. *Phys. Rev. B: Condens. Matter Mater. Phys.* **2000**, *61*, 7459.
(9) Kormann, C.; Bahnemann, D. W.; Hoffmann, M. R. *J. Phys. Chem.* **1988**, *92*, 5196.
(10) Fox, M. A. *Top. Curr. Chem.* **1987**, *142*, 71.
(11) Gerischer, H.; Heller, A. *J. Phys. Chem.* **1991**, *95*, 5261.
(12) Photocatalytic Purification and Treatment of Water and Air. In *Trace Met. Environ.* **1993**, *3*, Proceedings of the 1st International Conference on TiO Photocatalytic Purification and Treatment of Water and Air, London, Ontario, Canada, November 8−13, 1992; Ollis, D. F.; Al-Ekabi, H., Eds.
(13) *Photocatalysis: Fundamentals and Applications*; Serpone, N.; Pelizzetti, E.; Eds. Wiley: New York, 1989.
(14) O'Regan, B.; Graetzel, M. *Nature (London)* **1991**, *353*, 737.
(15) Nasr, C.; Liu, D.; Hotchandani, S.; Kamat, P. V. *J. Phys. Chem.* **1996**, *100*, 11054.
(16) Meyer, G. J. *J. Chem. Educ.* **1997**, *74*, 652.
(17) Ellingson, R. J.; Asbury, J. B.; Ferrere, S.; Ghosh, H. N.; Sprague, J. R.; Lian, T.; Nozik, A. J. *Z. Phys. Chem. (Muenchen)* **1999**, *212*, 77.
(18) Rehm, J. M.; McLendon, G. L.; Nagasawa, Y.; Yoshihara, K.; Moser, J.; Gratzel, M. *J. Phys. Chem.* **1996**, *100*, 9577.
(19) Doung, H. D.; Serpone, N.; Gratzel, M. *Helv. Chim. Acta*, **1984**, *67*, 1012.

(20) Rajh, T.; Nedeljkovic, J. M.; Chen, L. X.; Poluektov, O.; Thurnauer, M. C. *J. Phys. Chem. B* **1999**, *103*, 3515.
(21) Thurnauer, M. C.; Rajh, T.; Tiede, D. M. *Acta Chem. Scand.* **1997**, *51*, 610.
(22) Rabani, E.; Hetenyi, B.; Berne, B. J.; Brus, L. E. *J. Chem. Phys.* **1999**, *110*, 5355.
(23) Rajh, T.; Ostafin, A. E.; Micic, O. I.; Tiede, D. M.; Thurnauer, M. C. *J. Phys. Chem.* **1996**, *100*, 4538.
(24) Chen, L. X.; Rajh, T.; Wang, Z.; Thurnauer, M. C. *J. Phys. Chem. B* **1997**, *101*, 10688.
(25) Brusov, K. N.; Usyarov, O. G. *Kolloidn. Zh.* **1988**, *50*, 627.
(26) Milonjic, S. K.; Vucic, N. B.; Vujosevic, S. I. *Sep. Sci. Technol.* **1996**, *31*, 1515.
(27) Baes, C. F. M.; Robert E. *The Hydrolysis of Cations*; Wiley: New York, 1976.
(28) Rosenthal, J.; Yarmus, L. *Rev. Sci. Instrum.* **1966**, *37*, 381.
(29) Bresgunov, A. Y.; Dubinski, A. A.; Poluektov, O. G.; Vorb'eva, G. A.; Lebedev, Y. S. *J. Chem. Soc., Faraday Trans.* **1990**, *89*, 3185.
(30) Chen, L. X.; Liu, T.; Thurnauer, M. C.; Csencsits, R.; Rajh, T. *J. Phys. Chem. B*, submitted for publication, 2002.
(31) Nozik, A. J. *Annu. Rev. Phys. Chem.* **1978**, *29*, 189.
(32) Chen, L. X.; Rajh, T.; Jager, W.; Nedeljkovic, J.; Thurnauer, M. C. *J. Synchrotron Radiat.* **1999**, *6*, 445.
(33) Rajh, T.; Vucemilovic, M. I.; Dimitrijevic, N. M.; Micic, O. I.; Nozik, A. J. *Chem. Phys. Lett.* **1988**, *143*, 305.
(34) Atkins, P. W. *Physical Chemistry,* 2nd ed.; Oxford University Press: New York, 1978; p 775.
(35) Bogaris, B. A.; Cooper, S. R.; Koh, Y. B.; Raymond, K. N. *Inorg. Chem.* **1984**, *23*, 1009.
(36) Huber, R.; Sporlein S.; Moser, J. E.; Gratzel, M.; Wachtvetl, J. *J. Phys. Chem. B*. **2000**, *104*, 8995.
(37) Liu, T.; Chen, L. X.; Rajh, T. To be submitted for publication.
(38) Wu, Z. Y.; Ouvrard, G.; Gressier, P.; Natoli, C. R. *Phys. Rev. B* **1997**, *55*, 10382.
(39) Little, L. H. *Infrared Spectra of Adsorbed Species*; Academic Press: London, 1966.
(40) Lin-Vlen, D.; Colthup, N. B.; Fataley, W. G.; Grasselli, J. G. *The Handbook of Infrared Characteristic Frequencies of Organic Molecules*; Academic Press: London, 1991.
(41) Redfern, P.; Zapol, P.; Curtis, L.; Rajh, T.; Thurnauer, M. C., submitted for publication.
(42) Rajh, T.; Tiede, D. M.; Thurnauer, M. C. *J. Non-Cryst. Solids* **1996**, *205−207*, 815.
(43) Maron, S. H.; Lando, J. B. *Fundamentals of Physical Chemistry*; Macmillan Publishing: New York, 1974.
(44) Rodriguez, R.; Blesa, M. A.; Regazzoni, A. E. *J. Colloid Interface Sci.* **1996**, *177*, 122.
(45) Moser, J.; Punchihewa, S.; Infelta, P. P.; Gratzel, M. *Langmuir* **1991**, *7*, 3012.
(46) Liu, Y.; Dadap, J. I.; Zimdars, D.; Eisenthal, K. B. *J. Phys. Chem. B* **1999**, *103*, 2480.
(47) Fillinger, A.; Parkinson, B. *J. Electrochem. Soc.* **1999**, *146*, 4559.
(48) This refers to, on average, the *xz* plane of one unit cell that contains two Ti atoms and has an area of $9.37 \times 2.73 = 34.95$ Å^2. The other surface area *xy* has on average one Ti atom and a surface area of 13.9 Å^2. Assuming that in a colloid particle 50% adopt the *xy* plane and 50% adopt the *xz* plane the average surface area is $(17.5 + 13.9)/2 = 15.7$ Å^2.
(49) Chen, C.; Li, X.; Ma, W.; Zhao, J.; Hidaka, H.; Serpone, N. *J. Phys. Chem. B* **2002**, *106*, 318.
(50) Rajh, T.; Poluektov, O.; Dubinski, A. A.; Wiederrecht, G.; Thurnauer, M. C.; Trifunac, A. D. *Chem. Phys. Lett.* **2001**, *344*, 31.
(51) Dimitrijevic, N. M.; Bartels, D. M.; Trifunac A. D.; Rajh, T. To be submitted for publication.
(52) Felix, C. C.; Sealy, R. C. *J. Am. Chem. Soc.* **1982**, *104*, 1555.
(53) Stone, A. J. *Mol. Phys.* **1964**, *7*, 311.
(54) Stone, A. J. *Mol. Phys.* **1963**, *6*, 509.
(55) Anpo, M.; Shima, T.; Fujii, T.; Suzuki, S.; Che, M. *Chem. Lett.* **1987**, 1997.
(56) Howe, R. F.; Gratzel, M. *J. Phys. Chem.* **1985**, *89*, 4495.
(57) Meriaudeau, P.; Che, M.; Gravelle, P. C.; Teichner, S. J. *Bull. Soc. Chim. Fr.* **1971**, 13.
(58) Kerssen, J.; Volger, J. *Physica (Utrecht)* **1973**, *69*, 535.
(59) Shim, M.; Guyot-Sionnest, P. *J. Am. Chem. Soc.* **2001**, *123*, 11651.